Dendrite-Free Nanostructured Anode: Entrapment of Lithium in a 3D Fibrous Matrix for Ultra-Stable Lithium–Sulfur Batteries

*Xin-Bing Cheng, Hong-Jie Peng, Jia-Qi Huang, Fei Wei, and Qiang Zhang**

The lithium-ion batteries (LIBs) based on rocking-chair concept between intercalated cathode/anode pairs have achieved great success in the market of smartphones and laptops.[1] However, although the replacement of metallic lithium (Li) with graphite enhanced the safety of the lithium ion cells, it also significantly lowers the specific capacity and energy density, which is below the US Department of Energy Vehicle Technologies Program's long-term target for the secondary batteries.[2] Therefore, besides the successful commercialization of graphite anode, the academic research in metallic Li anode has never been in a sluggish during the past 40 years[3] to realize the ultimate replacement of internal combustion vehicles by electric vehicles. In fact, the Li metal is considered as the "Holy Grail" of energy storage systems due to its extremely high theoretical specific capacity (3860 mAh g^{-1}), low gravimetric density (0.59 g cm^{-3}), and lowest negative redox potential (–3.040 V *vs.* standard hydrogen electrode). Thus, Li metal exhibits superior theoretical performance than any other anode materials (such as silicon,[4] germanium (Ge),[5] metal oxides/sulfides,[6] nanocarbons,[7] and their composites,[8] etc.). The bright prospects give rise to worldwide interests in the metallic Li for the next generation energy storage systems, including highly considered rechargeable metallic Li batteries such as Li-O_2 and Li-sulfur (Li–S) batteries.

However, the formation of Li dendrites induced by inhomogeneous distribution of current density on the Li metal anode and the concentration gradient of Li ions at the electrolyte/electrode interface is a crucial issue that hinders the practical demonstration of high-energy-density metallic Li batteries.[9–12] On one hand, Li dendrites may pierce the polymer separator, resulting in short circuit and subsequent thermal runaway of the cell. Meanwhile, the growth of Li dendrites also leads to the formation of incomplete solid electrolyte interfaces (SEI), exposure of fresh Li to electrolytes, and the re-formation of thicker SEI films. Since SEI film is ionic conductive and electrical insulative, the resistance becomes larger as dendrites formed. During SEI formation, bare Li is continuously consumed, which decreases the cyclic efficiency of the whole cell. On the other hand, the dendrited Li possesses higher reactivity than plate Li. During the de-lithiation, the bottom of the Li dendrites prefers to lose Li first, rapidly dissolves at the local region, and breaks away from the anode,[13] leading to the formation of "dead Li" that is detached from the current collector and contributes no capacity. This also lowers the efficiency and stability of lithium anode in metallic Li batteries.

The composition, properties, and stability of the surface layer on Li, as well as the morphology of re-deposited Li are key factors that determine the cell performance of metallic Li batteries. If the stability and uniformity of the interfaces between electrolytes and Li electrode can be improved, the dendrite formation and growth would be retarded accordingly.[14] Various electrolyte additives (such as carbon dioxide/sulfur dioxide, hydrogen fluoride, 2-methylfuran, etc.)[12] with higher reduction voltages than solvents and salts are often employed to reinforce the interfaces on the Li metal. They react with Li anode quickly, form a dense and protective interphase, which further minimizes severe parasitic reactions between Li and electrolytes. Recently, low concentrations of cesium (Cs) or rubidium (Rb) ions with lower reduction potential than standard Li/Li^+ were employed to restrain the dendrite growth *via* self-healing electrostatic shield with positive charge formed around the Li protuberances to prevent further growth of dendrite, in which Cs or Rb cations cannot be consumed during Li deposition due to the lower reduction potential and thus remain effective even after long-term cycling.[11] Except for *in-situ* formed SEI films to protect Li anode, *ex-situ* coated polymer layers have been proposed to block dendrite penetration by physical confinement.[15] The ionic-liquid-nanoparticle hybrid electrolytes[16] and nanoporous polymer-ceramic composite electrolytes[17] with electrochemical stability, mechanical properties, and ability to promote stable Li electrodeposition are efficient in suppressing dendrite formation on cycled Li anodes. Thus, the growth behavior of Li dendrites has been effectively tuned by aforementioned strategies in liquid electrolytes. If organic electrolytes are replaced by polymer electrolytes (*e.g.* poly(ethylene oxide),[2,18] gel polymer electrolytes[19], all-solid-state electrolytes (*e.g.* nitrogen-doped Li-ion phosphate film,[20] ceramic glass,[21] and lithium thiophosphate based superionic conductors[22] with large shearing modulus, high

X.-B. Cheng, H.-J. Peng, Dr. J.-Q. Huang, Prof. F. Wei, Prof. Q. Zhang
Beijing Key Laboratory of Green Chemical Reaction Engineering and Technology
Department of Chemical Engineering
Tsinghua University
Beijing 100084, PR China
E-mail: zhang-qiang@mails.tsinghua.edu.cn

DOI: 10.1002/smll.201401837

mechanical strength, and noninflammability, the Li dendrite is expected to be fully suppressed under high stress strain.[23] However, the polymer-based and all-solid-state electrolytes possess much lower ionic conductivities than liquid electrolytes at room temperature and ultrahigh interfacial resistance due to the poor wettability to active phase. Consequently, the as-prepared LIBs with solid electrolytes can only be operated at over 60 °C (the melting point of PEO) for acceptable cell performance, which is suitable for stationary applications such as smart grids but difficult for electrical transportation pursuing high-power capability. Compared with these top-down strategies involving sophisticated considerations, bottom-up route with rational architectural design of metallic anode materials is another efficient method to mediate the growth behavior of deposited Li during charge-discharge process, which sheds a new light on the understanding of Li dendrite formation and provides a promising nanostructured metallic Li-based anode for high-energy-density rechargeable batteries.

Generally, Li metal is widely employed as the anode of Li batteries. As a 2D material without micro-/nanostructure, Li metal anode confronts the deadly risk of dendrite growth. Herein, we proposed a novel three-dimensional (3D) nanostructured anode with metallic Li contained in fibrous Li_7B_6 matrix (**Figure 1**a) as promising anode materials to prevent the dendrite growth. Comparing with other microstructured anode materials,[24] the nanostructured anode is with a large specific area, which reduces the current density to suppress the dendrite growth[25] (Figure 1b**,** the calculation principle is detailed described in Supporting Information). However, once the Li deposit initiates, it would grow continuously because Li deposit in the initial time is with a small size that holds a strong electric field strength, thus favoring the adsorption and deposition of lithium ions (Figure 1b). When the Li deposit size is beyond that of the matrix, Li^+ adsorption and deposition ability of the deposits will be below the matrix and then Li^+ deposits on the matrix rather than on the dendrites continually. Thus, the nanostructured LiB alloy anode not only reduces the current density, which decreases the growth velocity of Li deposits, but also limits the final size of deposited Li on the nanostructured matrix, which leads to the dendrite-free morphology at macroscale (Figure 1c). Consequently, the Li deposits on the nanostructured anode with metallic Li embeded in fibrous Li_7B_6 matrix are always with smaller size than that on the plate Li metal anode. Beyond the size effect of the Li deposits, the 3D fibrous structure of Li_7B_6 provides free space to accommodate electrolyte to reduce the concentration gradient of Li ions,[26] therefore, the formation of Li dendrites is suppressed. The 3D nanostructured anode with dendrite-free morphology and highly stable interfaces between the electrode and electrolyte could serve as a promising anode candidate for high-energy-density systems with good security.

The nanostructured anode with metallic Li contained in fibrous Li_7B_6 matrix reported herein is fabricated from thermal reaction and composed of free Li and alloyed Li with chemical formula of $Li_7B_6{\cdot}7.6Li$. The electrochemical phase evolution and corresponding structural properties of nanostructured anode at different charge/discharge stages were probed. A cell configuration of nanostructured anode as the working electrode, plate Li metal as the counter and reference electrode in the carbonate ester-based electrolyte (the composition was described in the Experimental Section) was constructed for electrochemically driving the phase evolution of nanostructured anode with metallic Li entrapped in fibrous Li_7B_6 matrix under a galvanostatic current density of 0.3 mA cm^{-2}, elaborating the multi-step and multi-phase de-lithiation and lithiation behaviors (**Figure 2**a). The initial plateau of around 30 mV observed in the first charge curve is attributed to the dissolution of free Li coated on the interconnected fibrous Li_7B_6 framework. The following phase evolution triggered by a huge uptake of voltage to plateau

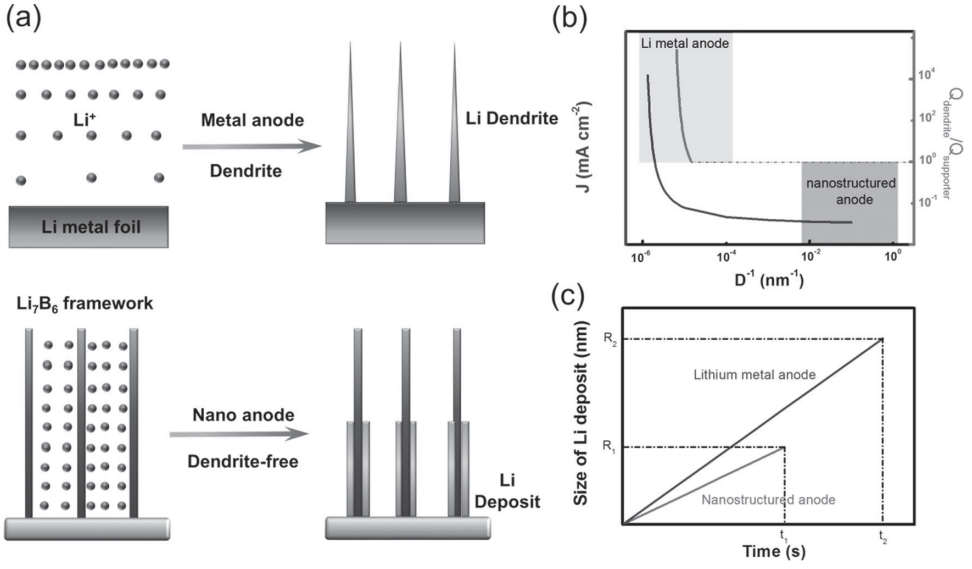

Figure 1. (a) Schematic illustrations of Li dendrite growth on the plate Li metal and Li deposits on nanostructured anode with metallic Li contained in fibrous Li_7B_6 matrix. (b) The relationship between the current density (J)/relative electric field strength ($Q_{dendrite}/Q_{supporter}$) to dendrite-Li and matrix size. (c) The size-time dependence of Li deposits on the nanostructured and plate Li anode, t_1, t_2, R_1, R_2 were the cut-off time of dendrite-Li growth and max size of Li dendrites on the nanostructured and plate Li metal anode, respectively ($t_1 < t_2$, $R_1 < R_2$).

small NANO MICRO

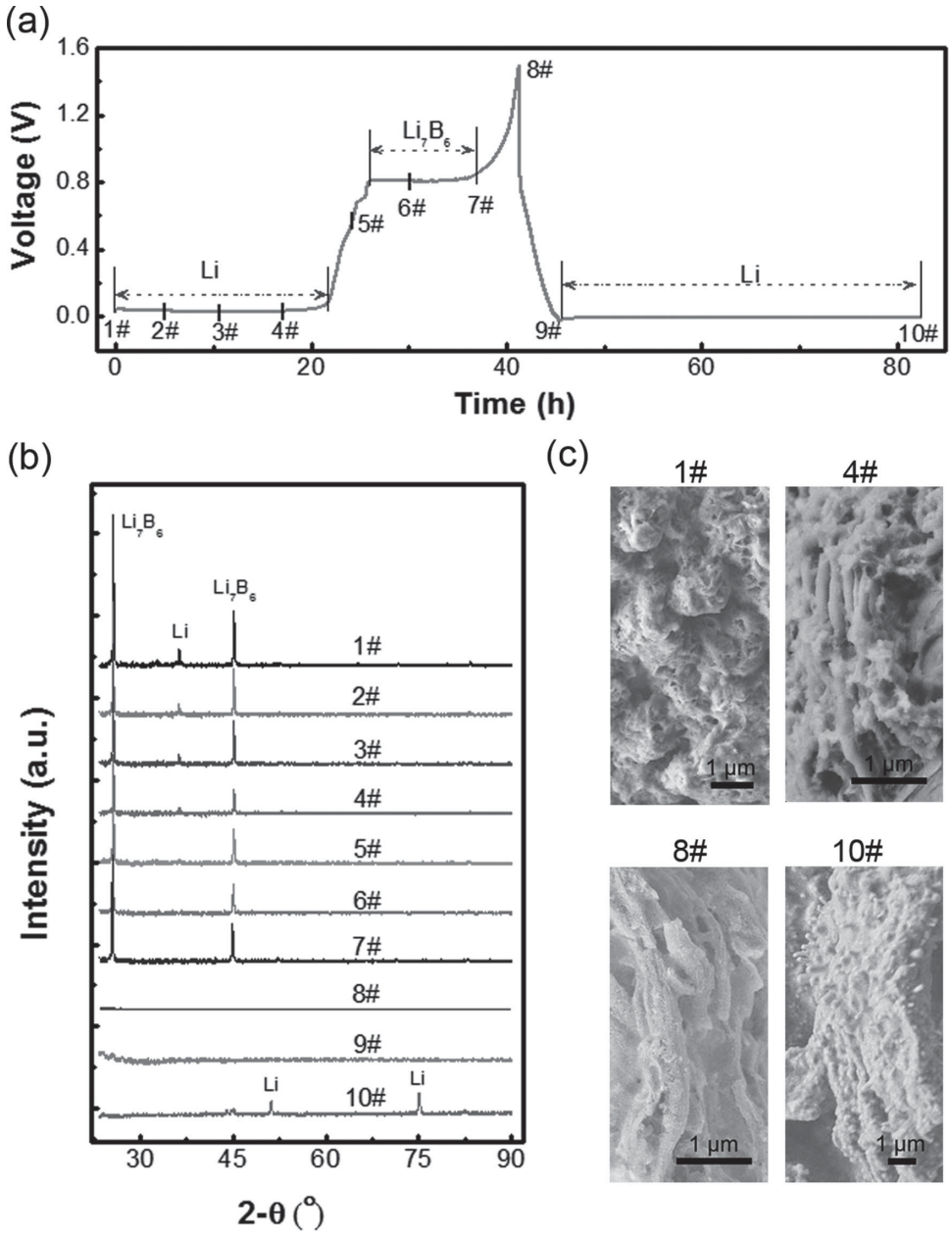

Figure 2. (a) Typical galvanostatic charge/discharge behavior of nanostructured anode with metallic Li contained in fibrous Li_7B_6 matrix at a current density of 0.3 mA cm^{-2} with plate Li metal as counter electrode. (b) XRD patterns and (c) corresponding SEM images of nanostructured anode during phase evolution denoted as 1#, 4#, 8#, and 10# in (a).

of 0.80 V corresponds to the extraction of combined Li from the Li_7B_6 phase. However, there is only one plateau around 5 mV in the lithiation process, indicating that the Li ions could not be alloyed with B to recover Li_7B_6 phase at room temperature.[27] This proposed structural evolution of nanostructured anode at different charge-discharge stages (denoted as 1#–10# in the galvanostatic profile) was confirmed by *ex-situ* X-ray diffraction (XRD) and scanning electron microscopy (SEM) analysis (Figure 2b,c). The initial nanostructured anode is composed of free Li and Li_7B_6 with the fibrous Li_7B_6 frameworks fully covered by free Li occupying the interspace of Li_7B_6 fibers (1#). With the de-lithiation, the peak of Li becomes weak (2#-4#) and after complete depletion of free Li as galvanostatic profile indicated, the XRD reflection of free Li disappears and the fibrous Li_7B_6 with a diameter of 100–200 nm gradually exposed (5#). With deep de-lithiation to fully extract Li in Li_7B_6 phase (6#, 7#), amorphous B phase remained with well-preserved fibrous morphology and diameter, illustrating the structure stability of Li_7B_6/B scaffold (8#). During the subsequent lithiation (9#, 10#), only free Li with lower crystallization and corresponding smaller size of around 100–300 nm deposits on the inert B skeleton while no crystallized Li_7B_6 phase is generated (10#).[27] When Li ions are reduced at the surface of such inert scaffold, the deposition of free Li could only be initiated at the current collector side to accept sufficient electrons and then epitaxy of Li on B develops to membrane side since the free Li is conductive. Both the nanostructured fibrous Li_7B_6 and B framework

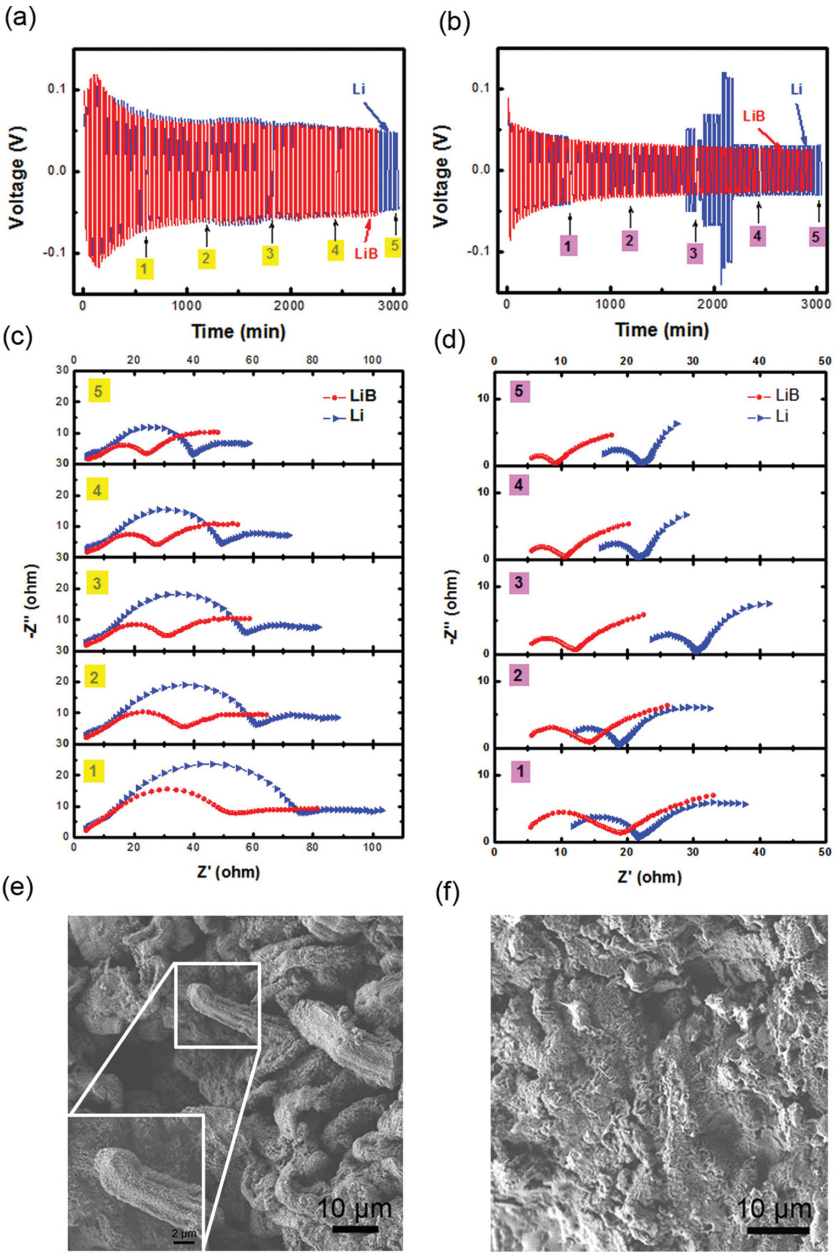

Figure 3. The electrode interface dynamics of nanostructured anode with metallic Li contained in fibrous Li_7B_6 matrix in comparison with plate Li metal anode in symmetrical cells. (a,b) Interface stabilities during cycling and (c,d) electrochemical impedance spectroscopy (EIS) profiles after different cycles showing interface resistance when carbonate ester-based and polysulfide-containing electrolytes were employed, respectively. The morphologies of (e) plate Li metal and (f) nanostructured electrodes after charging at a current density of 10 mA cm^{-2} for 40 h.

have enough space for efficient deposition of free Li. Compared to pure B framework, combined Li_7B_6 possesses higher electrical conductivity to serve as highly efficient electron pathways and thus more ideal nanostructured anode scaffold without dendrite issues if the charging potential is limited to lower than 0.80 V in practical applications for high-energy-density systems.

The stabilities of both electrode/electrolyte interface and interfacial transfer behavior are pivotal for the high efficient cycling of metal anode. Symmetrical cells are always employed to investigate the interfacial behaviors of metal anodes.[28] Herein, two symmetrical cells of plate Li metal or nanostructured metallic Li anodes in combination with two electrolytes of carbonate ester-based electrolyte and polysulfide electrolyte (the composition was described in Experimental Section) were fabricated to simulate the interfacial stability and transfer phenomena in Li-ion battery and Li-S battery applications, respectively. The carbonate ester electrolyte is commonly used for Li-ion battery due to its effectiveness to build a stable interface at the anode surface. Therefore, both nanostructured metallic Li and plate Li metal electrodes exhibit low voltage fluctuation (**Figure 3**a). However, nanostructured metallic Li electrode displays ameliorative polarization and much lower impedance than plate Li metal electrode during the whole cycling course, indicating superior transfer properties at the interface (Figure 3c). The rapid electron transfer is attributed to the long-range conductive fibrous Li_7B_6 framework, while the interconnected hierarchical pores among the 3D scaffolds benefit the fully penetration of electrolytes and fast ion diffusion. Considering the applications in Li-S batteries, in which highly reactive Li easily reduces the soluble intermediates in form of polysulfides into insoluble and insulative Li_2S covering the anode surface to cause loss of active material and high interfacial resistance as a key issue,[29] the replacement of plate metallic Li anode is urgent. In polysulfide electrolytes, metallic Li exhibits an irregular potential fluctuation and high impedance due to the complex reaction between polysulfides and Li metal to form inhomogeneous deposited electron/ion inhibitor of Li_2S as high transfer barrier with poor polarization (Figure 3b,d). While nanostructured metallic Li electrodes shows regular polarization curves and much lower resistance, suggesting a stable and thin interface is formed on nanosized Li embedded in fibrous framework. This can be ascribed to lower concentration gradient of both Li ions and polysulfides to suppress Li_2S growing into bulk insulating phase. Consequently, the LiB electrode is highly considered to replace metallic Li anode in Li-S batteries for superior cell performance and stability.

The 3D nanostructured anode with metallic Li contained in fibrous Li_7B_6 matrix not only afford favorable interfacial stability and transfer properties, but also suppress the dendrite growth due to decreased areal current density and local

small NANO MICRO

concentration gradient of Li ions. Large Li dendrites are not available for both plate Li metal and nanostructured metallic Li electrodes at a low current density of 0.3 mA cm^{-2}, while the surface of plate Li metal is more coarse than nanostructured metallic Li anode (Figure S1).[25] However, a large quantity of micro-sized Li dendrites is observed in case of plate Li metal anode while the nanostructured metallic Li anode is dendrite-free when applying a huge current density of 10 mA cm^{-2} based on the surface of flat electrode (Figure 3e, f). For plate Li metal electrode, the huge uptake of current results in strong local electrical field and extremely high concentration gradient of Li ions as driven force for high throughput transportation of electrons from electrode and ions from electrolyte, which is beneficial for the dendrite growth. While for the nanostructured metallic Li anode, its 3D nanostructure with abundant electrode/electrolyte interfaces lower the absolute local current density even though applying the same current as Li anode. Thus both the gradients of electrical field and Li ion concentration at local regions are reduced to orders of magnitude towards increased Sand's time and dendrite-free morphology.[9,30] Also, due to the nanosized matrix, the growth of Li crystal is also self-restricted in principles shown in Figure 1. The dendrite-free 3D nanostructured anode with metallic Li contained in fibrous Li_7B_6 matrix circumvents the safety issue of next generation of energy storage systems with metal anodes (*e.g.* rechargeable Li–O_2 and Li–S batteries) for a bright prospect.

With a theoretical capacity of 1675 mAh g^{-1}, elemental S posing advantages of low cost, low toxicity, and abundant resource has been considered as one of the most promising alternative cathode materials. Its pair with metallic Li delivers ultrahigh theoretical energy density of 2567 Wh kg^{-1}, which is, however, hindered by low utilization of S and loss of active materials through dissolution of polysulfides and their parasitic reaction with Li anode. To date, the utilization of S and dissolution of polysulfides have been well addressed by various nanostructured cathode materials.[31] However, rare investigation on anode side, especially nanostructured Li anodes, has been developed to circumvent the aforementioned parasitic reaction issue of Li-S chemistry and dendrite problem like other metallic-Li batteries,[32] though several non-metal-based Li anodes were employed.[33] However, the critical role of the nanostructure on the morphology and electrochemical performance of the metallic Li anode was not well understood yet. Herein, the nanostructured anode with metallic Li embeded in fibrous Li_7B_6 matrix is expected to be proof-of-concept of high security Li-S cells due to its stable interfacial properties and dendrite-free feature as well as low over potential *vs.* Li^+/Li.

The two-electrode Li-S cells to evaluate the practical potential of nanostructured anode were fabricated by employing carbon nanotube (CNT) based S composite cathode and routine lithium nitrate-free electrolyte (details were described in Experimental Section and our previous work[34]). Unprecedented cycling life extended to 2000 cycles, low cyclic degradation of 0.032%, and over two times higher retention than Li anode are achieved by nanostructured anode (**Figure 4**a and Figure S2). More importantly, the

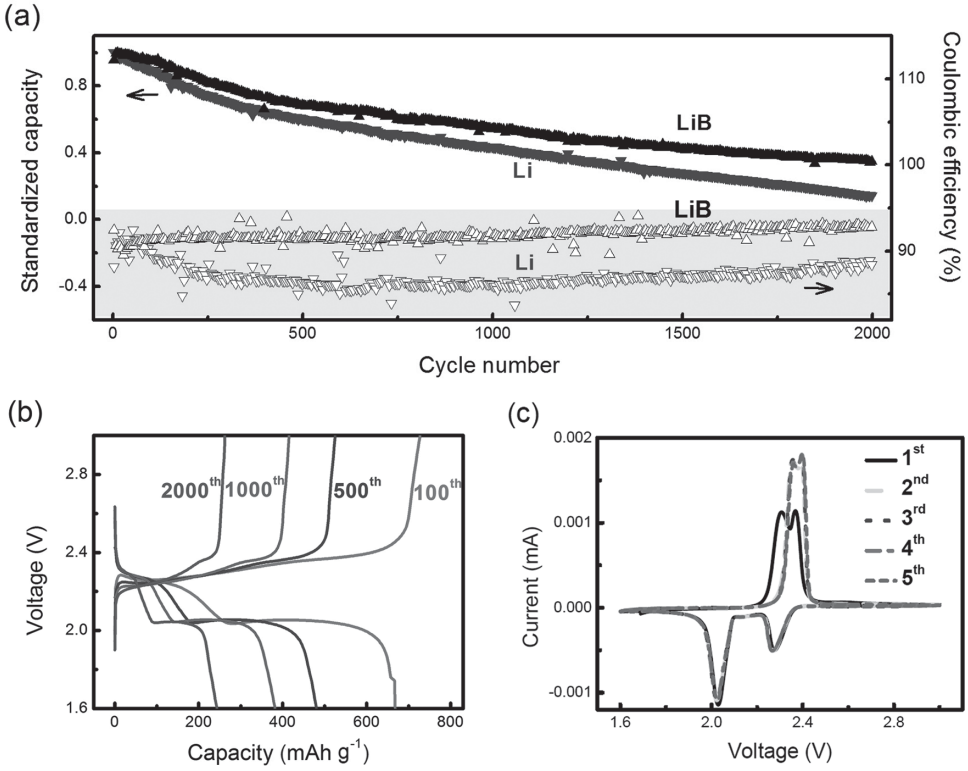

Figure 4. The electrochemical performance Li-S batteries employing nanostructured anode. (a) Long-term cycling performance with nanostructured metallic Li anode and plate Li metal anode at a current density of 1.0 C (1.0 C = 1675 mAh g^{-1}) and (b) corresponding galvanostatic charge-discharge profiles of cell with nanostructured metallic Li anode; (c) the CV curves of nanostructured metallic Li anode with S composite cathode as the working electrode at a scan rate of 0.1 mV s^{-1}.

coulombic efficiency remains 91–92% during the long-term cycling due to the stable interfacial properties of nanostructured surface, which is much higher and more stable than that of the cell with Li anode. The high efficiency is pivotal for conducting a practical device with low thermal throughput, combining with dendrite-free feature to guarantee high security. In the typical galvanostatic charge-discharge curves involving multi-electron-transfer chemistry, Li-S battery with nanostructured anode retains discharge plateaus around 2.06 V during 2000 cycles, indicating the stable transformation reactions (Figure 4b). In contrast, the voltage of cells with Li anode fades significantly in 2000 cycles, which is ascribed to the inhomogeneous deposition Li_2S blocking efficient mass and charge transfer to retard favorable electrode kinetics (Figure S3). The stable electrochemical reaction beneficial from the nanostructure of LiB anode is also demonstrated by almost unchanged position and strength of redox peaks in cyclic voltammetry (CV) profiles after initial activation in the first cycle (Figure 4c). Furthermore, the robust fibrous morphology of LiB anode is well preserved after 2000 cycles while many protuberances are observed on the cycled Li anode, which may possibly pierce the separator during prolonged cycles and induce hazardous risks (Figure S4). Nanostructured metallic Li anode demonstrates high efficiency, stable performance, and huge potential for high security Li-S batteries with high energy density.

In summary, we engineered the 3D nanostructured electrode with metallic Li contained in fibrous Li_7B_6 matrix as the anode materials of high-energy-density metallic Li-S batteries, which demonstrate unprecedentedly stable long cycling performance and high coulombic efficiency beyond plate Li metal. The superior performance is attributed to unique 3D nanostructured Li_7B_6 framework, which not only decreases the areal current density by improved surface area, but also provided enough space to accommodate the electrolyte and re-deposited Li to stabilize the concentration of Li ions. Thus, nanostructured anodes maintain a stable interfacial behavior, reduce the transfer resistance, and inhibit the growth of Li dendrites. These favorable features render typical Li-S batteries based on nanostructured anode with high stability and efficiency, as well as unprecedented cycling life to 2000 cycles. Beyond Li-S batteries, the nanostructured anode with unique 3D nanostructure will shed a light on other advanced energy storage system involving metal anode, such as the Li-O_2 batteries and other metal-air battery, as well as next generation of Li batteries.

Experimental Section

Materials: The plate Li metal and nanostructured metallic anode with metallic Li contained in fibrous Li_7B_6 matrix fabricated from thermal reaction are commercially available form China Energy Lithium Co., Ltd. The carbonate ester based electrolyte is 1.0 M lithium hexafluorophosphate ($LiPF_6$) dissolving in a ternary solution of ethylene carbonate (EC) – dimethyl carbonate (DMC) – ethylene methyl carbonate (EMC) with a volumetric ratio of 1:1:1 and the ether based electrolyte employed for Li-S cell test is composed of lithium bis(trifluoromethanesulfonyl)imide (LiTFSI) (1.0 M) as solvate and 1,3-dioxolane (DOL)/1,2-dimethoxyethane (DME) with a volumetric ratio of 1:1. Both of the two electrolytes were purchased from Zhangjiagang Guotai Huarong Chemical New Material Co., Ltd. To prepare polysulfide electrolyte, elemental S and pure Li_2S purchased from Alfa Aesar were mixed in a stoichiometric proportion to obtain Li_2S_5 (0.1 M) dissolving in the ester based electrolytes. The CNTs were produced by chemical vapor deposition on Fe based catalyst in a fluidized bed reactor and routine purification by acid was carried out.[35]

Structure Characterizations: *Ex-situ* XRD and SEM experiments are conducted by an X-ray diffractor (XRD, D8-Advance, Bruker, Germany) and a scanning electron microscopy (SEM, JSM 7401F, JEOL Ltd., Tokyo, Japan) at 3.0 kV.

Electrochemical Measurement of Symmetrical Cells: A two-electrode cell configuration using standard 2025 coin-type cells was used here, which were assembled in an Ar-filled glove box with O_2 and water content below 1 ppm. The electrochemically driven phase evolution is achieved in cells with LiB as the cathode and Li as the anode using carbonate ester-based electrolyte. The symmetrical cells were fabricated with plate Li metal or nanostructured metallic Li in the carbonate ester-based electrolyte and polysulfide electrolyte, respectively. The galvanostatic mode, the CV (at a scan rate of 0.1 mV s^{-1}) and EIS measurements (frequency range of 10^{-2} – 10^5 Hz) were performed on Solartron 1470E electrochemical workstation.

Electrochemical Evaluation of Li-S Batteries: The fabrication of cathode materials and electrodes is demonstrated elsewhere.[34] The content of S is 64 wt% in the CNT@S composites. The CNT@S slurry was then coated onto an Al foam, which was punched into 13.0 mm disks with an areal loading of 4.6 mg cm^{-2}. Note that the electrolyte is lithium nitrate-free.

Supporting Information

Supporting Information is available from the Wiley Online Library or from the author.

Acknowledgements

The authors thank Hong-Xia Yuan and Jing Wang for their help in XRD experiments. This work was supported by Natural Scientific Foundation of China (No. 21306103) and the China Postdoctoral Science Foundation (2012M520293, 2013T60125).

[1] a) J. W. Long, B. Dunn, D. R. Rolison, H. S. White, *Chem. Rev.* **2004**, *104*, 4463; b) J. Chen, F. Cheng, *Accounts. Chem. Res.* **2009**, *42*, 713.
[2] R. Khurana, J. Schaefer, L. A. Archer, G. W. Coates, *J. Am. Chem. Soc.* **2014**, *136*, 7395.
[3] a) M. S. Whittingham, *Proc. IEEE* **2012**, *100*, 1518; b) D. Aurbach, Y. Cohen, *J. Electrochem. Soc.* **1996**, *143*, 3525.
[4] a) C. Wang, H. Wu, Z. Chen, M. T. McDowell, Y. Cui, Z. Bao, *Nat. Chem.* **2013**, *5*, 1042; b) N. Liu, Z. Lu, J. Zhao, M. T. McDowell, H.-W. Lee, W. Zhao, Y. Cui, *Nat. Nanotechnol.* **2014**, *9*, 187; c) X. Huang, J. Yang, S. Mao, J. Chang, P. B. Hallac, C. R. Fell, B. Metz, J. Jiang, P. T. Hurley, J. Chen, *Adv. Mater.* **2014**, *26*, 4326.

small NANO MICRO

[5] L. Yang, Q. Gao, L. Li, Y. Tang, Y. Wu, *Electrochem. Commun.* **2010**, *12*, 418.

[6] a) P. Poizot, S. Laruelle, S. Grugeon, L. Dupont, J. M. Tarascon, *Nature* **2000**, *407*, 496; b) A. S. Arico, P. Bruce, B. Scrosati, J. M. Tarascon, W. Van Schalkwijk, *Nat. Mater.* **2005**, *4*, 366.

[7] a) D. Pan, S. Wang, B. Zhao, M. Wu, H. Zhang, Y. Wang, Z. Jiao, *Chem. Mater.* **2009**, *21*, 3136; b) T. Bhardwaj, A. Antic, B. Pavan, V. Barone, B. D. Fahlman, *J. Am. Chem. Soc.* **2010**, *132*, 12556; c) S. Y. Yin, Y. Y. Zhang, J. H. Kong, C. J. Zou, C. M. Li, X. H. Lu, J. Ma, F. Y. C. Boey, X. D. Chen, *ACS Nano* **2011**, *5*, 3831.

[8] a) S. Yang, G. Cui, S. Pang, Q. Cao, U. Kolb, X. Feng, J. Maier, K. Müllen, *ChemSusChem* **2010**, *3*, 236; b) H. Wang, L.-F. Cui, Y. Yang, H. Sanchez Casalongue, J. T. Robinson, Y. Liang, Y. Cui, H. Dai, *J. Am. Chem. Soc.* **2010**, *132*, 13978.

[9] a) J.-N. Chazalviel, *Phys. Rev. A* **1990**, *42*, 7355; b) M. Rosso, T. Gobron, C. Brissot, J.-N. Chazalviel, S. Lascaud, *J. Power Sources* **2001**, *97*, 804.

[10] a) M. Rosso, C. Brissot, A. Teyssot, M. Dollé, L. Sannier, J.-M. Tarascon, R. Bouchet, S. Lascaud, *Electrochim. Acta* **2006**, *51*, 5334; b) R. Bouchet, S. Maria, R. Meziane, A. Aboulaich, L. Lienafa, J.-P. Bonnet, T. N. Phan, D. Bertin, D. Gigmes, D. Devaux, *Nat. Mater.* **2013**, *12*, 452.

[11] F. Ding, W. Xu, G. L. Graff, J. Zhang, M. L. Sushko, X. Chen, Y. Shao, M. H. Engelhard, Z. Nie, J. Xiao, *J. Am. Chem. Soc.* **2013**, *135*, 4450.

[12] W. Xu, J. Wang, F. Ding, X. Chen, E. Nasybulin, Y. Zhang, J.-G. Zhang, *Energy Environ. Sci.* **2014**, *7*, 513.

[13] M. Arakawa, S.-i. Tobishima, Y. Nemoto, M. Ichimura, J.-i. Yamaki, *J. Power Sources* **1993**, *43*, 27.

[14] a) K. Xu, *Chem. Rev.* **2004**, *104*, 4303; b) Z. Zeng, W.-I. Liang, H.-G. Liao, H. Xin, Y.-H. Chu, H. Zheng, *Nano Lett.* **2014**, *14*, 1745.

[15] a) G. A. Umeda, E. Menke, M. Richard, K. L. Stamm, F. Wudl, B. Dunn, *J. Mater. Chem.* **2011**, *21*, 1593; b) R. S. Thompson, D. J. Schroeder, C. M. López, S. Neuhold, J. T. Vaughey, *Electrochem. Commun.* **2011**, *13*, 1369; c) J. J. Woo, Z. Zhang, K. Amine, *Adv. Energy Mater.* **2014**, *4*, 1301208.

[16] a) Y. Y. Lu, S. K. Das, S. S. Moganty, L. A. Archer, *Adv. Mater.* **2012**, *24*, 4430; b) Y. Y. Lu, K. Korf, Y. Kambe, Z. Y. Tu, L. A. Archer, *Angew. Chem. Int. Ed.* **2014**, *53*, 488.

[17] Z. Y. Tu, Y. Kambe, Y. Y. Lu, L. A. Archer, *Adv. Energy Mater.* **2014**, *4*, 1300654.

[18] D. Payne, P. Wright, *Polymer* **1982**, *23*, 690.

[19] K. Abraham, M. Alamgir, *J. Electrochem. Soc.* **1990**, *137*, 1657.

[20] a) J. Bates, N. Dudney, G. Gruzalski, R. Zuhr, A. Choudhury, C. Luck, J. Robertson, *J. Power Sources* **1993**, *43*, 103; b) E. Herbert, W. E. Tenhaeff, N. J. Dudney, G. Pharr, *Thin Solid Films* **2011**, *520*, 413.

[21] a) J. Fu, *Solid State Ionics* **1997**, *96*, 195; b) V. Thangadurai, W. Weppner, *Adv. Funct. Mater.* **2005**, *15*, 107.

[22] a) N. Kamaya, K. Homma, Y. Yamakawa, M. Hirayama, R. Kanno, M. Yonemura, T. Kamiyama, Y. Kato, S. Hama, K. Kawamoto, A. Mitsui, *Nat. Mater.* **2011**, *10*, 682; b) Z. C. Liu, W. J. Fu, E. A. Payzant, X. Yu, Z. L. Wu, N. J. Dudney, J. Kiggans, K. L. Hong, A. J. Rondinone, C. D. Liang, *J. Am. Chem. Soc.* **2013**, *135*, 975.

[23] C. Monroe, J. Newman, *J. Electrochem. Soc.* **2005**, *152*, A396.

[24] J. Heine, S. Krüger, C. Hartnig, U. Wietelmann, M. Winter, P. Bieker, *Adv. Energy Mater.* **2014**, *4*, 1300815.

[25] a) C. Brissot, M. Rosso, J.-N. Chazalviel, P. Baudry, S. Lascaud, *Electrochim. Acta* **1998**, *43*, 1569; b) C. Brissot, M. Rosso, J. N. Chazalviel, S. Lascaud, *J. Electrochem. Soc.* **1999**, *146*, 4393.

[26] S. Chabi, C. Peng, D. Hu, Y. Zhu, *Adv. Mater.* **2014**, *26*, 2440.

[27] X. Ding, X. Lu, Z. Fu, H. Li, *Electrochim. Acta* **2013**, *87*, 230.

[28] a) G. H. Lane, A. S. Best, D. R. MacFarlane, M. Forsyth, A. F. Hollenkamp, *Electrochim. Acta* **2010**, *55*, 2210; b) J.-K. Kim, A. Matic, J.-H. Ahn, P. Jacobsson, *J. Power Sources* **2010**, *195*, 7639; c) S. Xiong, K. Xie, Y. Diao, X. Hong, *J. Power Sources* **2013**, *236*, 181.

[29] S. Xiong, K. Xie, Y. Diao, X. Hong, *J. Power Sources* **2014**, *246*, 840.

[30] V. Fleury, J.-N. Chazalviel, M. Rosso, B. Sapoval, *J. Electroanal. Chem. Interfacial Electrochem.* **1990**, *290*, 249.

[31] a) L. Xiao, Y. Cao, J. Xiao, B. Schwenzer, M. H. Engelhard, L. V. Saraf, Z. Nie, G. J. Exarhos, J. Liu, *Adv. Mater.* **2012**, *24*, 1176; b) G. Zhou, S. Pei, L. Li, D. W. Wang, S. Wang, K. Huang, L. C. Yin, F. Li, H. M. Cheng, *Adv. Mater.* **2014**, *26*, 625; c) S. Xin, L. Gu, N.-H. Zhao, Y.-X. Yin, L.-J. Zhou, Y.-G. Guo, L.-J. Wan, *J. Am. Chem. Soc.* **2012**, *134*, 18510; d) D. W. Wang, Q. C. Zeng, G. M. Zhou, L. C. Yin, F. Li, H. M. Cheng, I. R. Gentle, G. Q. M. Lu, *J. Mater. Chem. A* **2013**, *1*, 9382; e) Y. Yang, G. Zheng, Y. Cui, *Chem. Soc. Rev.* **2013**, *42*, 3018; f) M. Q. Zhao, Q. Zhang, J. Q. Huang, G. L. Tian, J. Q. Nie, H. J. Peng, F. Wei, *Nat. Commun.* **2014**, *5*, 3410; g) J. Song, T. Xu, M. L. Gordin, P. Zhu, D. Lv, Y.-B. Jiang, Y. Chen, Y. Duan, D. H. Wang, *Adv. Funct. Mater.* **2014**, *24*, 1243; h) J. T. Lee, Y. Y. Zhao, S. Thieme, H. Kim, M. Oschatz, L. Borchardt, A. Magasinski, W. I. Cho, S. Kaskel, G. Yushin, *Adv. Mater.* **2013**, *25*, 4573; i) L. Wang, Y. Zhao, M. L. Thomas, H. R. Byon, *Adv. Funct. Mater.* **2014**, *24*, 2248; j) H. J. Peng, J. Q. Huang, M. Q. Zhao, Q. Zhang, X. B. Cheng, X. Y. Liu, W. Z. Qian, F. Wei, *Adv. Funct. Mater.* **2014**, *24*, 2772; k) L. C. Yin, J. L. Wang, F. J. Lin, J. Yang, Y. Nuli, *Energy Environ. Sci.* **2012**, *5*, 6966; l) J. Bruckner, S. Thieme, F. Bottger-Hiller, I. Bauer, H. T. Grossmann, P. Strubel, H. Althues, S. Spange, S. Kaskel, *Adv. Funct. Mater.* **2014**, *24*, 1284; m) L. F. Xiao, Y. L. Cao, J. Xiao, B. Schwenzer, M. H. Engelhard, L. V. Saraf, Z. M. Nie, G. J. Exarhos, J. Liu, *Adv. Mater.* **2012**, *24*, 1176.

[32] H. Kim, G. Jeong, Y. U. Kim, J. H. Kim, C. M. Park, H. J. Sohn, *Chem. Soc. Rev.* **2013**, *42*, 9011.

[33] a) M. H. Miles, G. E. McManis, A. N. Fletcher, *Electrochim. Acta* **1985**, *30*, 889; b) P. Sanchez, C. Belin, C. Crepy, A. Deguibert, *J. Appl. Electrochem.* **1989**, *19*, 421; c) P. Sanchez, C. Belin, G. Crepy, A. Deguibert, *J. Mater. Sci.* **1992**, *27*, 240; d) A. Meden, B. Pihlar, S. Pejovnik, *J. Appl. Electrochem.* **1994**, *24*, 78; e) S. Liu, J. Yang, L. Yin, Z. Li, J. Wang, Y. Nuli, *Electrochim. Acta* **2011**, *56*, 8900; f) H. Kim, J. T. Lee, D. C. Lee, M. Oschatz, W. I. Cho, S. Kaskel, G. Yushin, *Electrochem. Commun.* **2013**, *36*, 38; g) B. Duan, W. Wang, H. Zhao, A. Wang, M. Wang, K. Yuan, Z. Yu, Y. Yang, *ECS Electrochemistry Letters* **2013**, *2*, A47; h) X. L. Zhang, W. K. Wang, A. B. Wang, Y. Q. Huang, K. G. Yuan, Z. B. Yu, J. Y. Qiu, Y. S. Yang, *J. Mater. Chem. A* **2014**, *2*, 11660.

[34] X.-B. Cheng, J.-Q. Huang, Q. Zhang, H.-J. Peng, M.-Q. Zhao, F. Wei, *Nano Energy* **2014**, *4*, 65.

[35] a) Q. Zhang, M. Q. Zhao, Y. Liu, A. Y. Cao, W. Z. Qian, Y. F. Lu, F. Wei, *Adv. Mater.* **2009**, *21*, 2876; b) Q. Zhang, M. Q. Zhao, J. Q. Huang, Y. Liu, Y. Wang, W. Z. Qian, F. Wei, *Carbon* **2009**, *47*, 2600.

Received: June 23, 2014
Published online: July 29, 2014

